Available online at www.sciencedirect.com
ScienceDirect
Acta Materialia 57 (2009) 5947–5955
Acta MATERIALIA
www.elsevier.com/locate/actamat

First-principles calculations of vacancy–solute element interactions in body-centered cubic iron

Toshiharu Ohnuma *, Naoki Soneda, Misako Iwasawa

Material Science Research Laboratory, CRIEPI, Central Research Institute of Electric Power Industry, 2-11-1 Iwado Kita, Komaeshi, Tokyo 201-8511, Japan

Received 22 August 2008; received in revised form 15 May 2009; accepted 10 August 2009
Available online 11 September 2009

Abstract

We have studied the vacancy–solute atom interactions in body-centered cubic Fe by means of first-principles calculations to obtain a better understanding of them for the application of ferritic steels, which are very important structural materials for fission and fusion reactors. The interactions between a vacancy and carbon/nitrogen interstitial atoms are studied in detail to obtain the binding energies and stable structures of the complexes. Substitutional atoms of 3d transition metals, such as Sc, Ti, V, Cr, Mn, Co, Ni, Cu and Zn, and of other important elements Si, P, S and Mo, are also studied to obtain their binding energies with a vacancy. The origin of the binding energies is discussed from the viewpoints of electronic structures and the distortion of the crystalline lattice.
© 2009 Acta Materialia Inc. Published by Elsevier Ltd. All rights reserved.

Keywords: Iron; Embrittlement; First-principles electron theory

1. Introduction

The high-energy particle irradiation of metals can produce point defects such as vacancies and self-interstitial atoms in the metal lattice. The diffusion of these defects causes fine microstructural changes in metals, which lead to macroscopic changes in their mechanical properties. The diffusion of vacancies is of particular interest because vacancies not only form clusters, voids or loops by themselves but also promote the diffusion of substitutional-type solute atoms in the matrix by a vacancy mechanism to cause the clustering, segregation and precipitation of the solute atoms. This process of solute diffusion is controlled by the strength of the interaction between a vacancy and the solute atom, whose magnitude depends on the element. On the other hand, it is also well known that the diffusion of vacancies is significantly influenced by the presence of interstitial-type solute atoms, which can exist in a vacancy to form a vacancy–interstitial atom complex. In this case, not only the vacancy–solute atom interaction but also solute–solute interactions in the vacancy are also very important. Thus, understanding the fundamental mechanisms of the vacancy–solute atom interactions is very important for developing predictive models of changes in the microstructure and mechanical properties of metals for engineering applications in fission and fusion reactors.

In this paper, we study the vacancy–solute atom interactions in body-centered cubic (bcc) Fe by means of first-principles calculations to obtain a better understanding of them for the application of ferritic steels, which are very important structural materials for fission and fusion reactors. The interactions between a vacancy and carbon/nitrogen interstitial atoms are studied in detail to obtain the binding energies and stable structures of the complexes. Substitutional atoms of 3d transition metals, such as Sc, Ti, V, Cr, Mn, Co, Ni, Cu and Zn, and of other important elements Si, P, S and Mo, are also studied to obtain their binding energies with a vacancy. The origin of the binding

* Corresponding author. Tel.: +81 3 3480 2111; fax: +81 3 3430 2410.
E-mail address: ohnuma@criepi.denken.or.jp (T. Ohnuma).

1359-6454/$36.00 © 2009 Acta Materialia Inc. Published by Elsevier Ltd. All rights reserved.
doi:10.1016/j.actamat.2009.08.020

energies is discussed from the viewpoints of electronic structures and the distortion of the crystalline lattice.

2. Calculation details

2.1. First-principles calculation

The VASP code is used in this study along with the combination of the generalized gradient approximation (GGA) for the exchange and correlation energies and density functional theory [1,2]. We used the projector augmented-wave method [3,4]. The cutoff energy of the plane waves is 400 eV. The unit cell is based on a $4 \times 4 \times 4$ bcc lattice, which contains 128 Fe atoms. The spin polarization effect is included to consider the magnetism of the bcc Fe crystal. In the calculation of the optimized structure, the unit cell shape, unit cell size and atomic configuration are relaxed using the stress tensor. Atomic configurations are further optimized using the Hellman–Feynman force. Brillouin zone integration is performed by the Monkhorst–Pack scheme with a $2 \times 2 \times 2$ mesh for relaxation and a $3 \times 3 \times 3$ mesh for single-point energy calculation.

The calculation scheme for vacancy–*n*-carbon (VC_n) complexes and vacancy–*n*-nitrogen (VN_n) complexes is as follows. Calculations start with the bcc Fe structure containing one vacancy associated with *n*-carbon (or nitrogen) atoms. The carbon atoms are placed at either the octahedral, tetrahedral or substitutional sites of the vacancy. The lattice constant of the Fe crystal is first set to the value calculated for the perfect bcc Fe crystal containing no vacancy. The atom positions as well as the lattice constant and the shape of the unit cell are optimized on the basis of the interatomic forces and stress tensors to achieve the lowest-energy configuration under a given pressure.

2.2. Energy calculations

To describe the equations used to calculate binding energies, we here introduce an expression, $E_c(\Lambda_{Conf}^{Atoms})$, where E_c denotes the total energy of a crystal with configuration Λ_{Conf}^{Atoms}, *Conf* is the type of defect in the crystal and *Atoms* indicates the atoms used in the energy calculation. For example, $E_c(\Lambda_{VX_n}^{Fe,X})$ denotes the total energy of the crystal containing a VX_n complex, where X is either C (carbon) or N (nitrogen), while $E_c(\Lambda_{VX_n}^{Fe})$ and $E_c(\Lambda_{VX_n}^{X})$ denote the energies of iron atoms only and X atoms only in the crystal containing a VX_n complex, respectively. Using this notation, we can write the total binding energy of VX_n, $E_b^T(VX_n)$, as follows:

$$E_b^T(VX_n) = \left\{E_c\left(\Lambda_V^{Fe}\right) + n \times E_c\left(\Lambda_X^{Fe,X}\right)\right\} - \left\{n \times E_c\left(\Lambda^{Fe}\right) + E_c\left(\Lambda_{VX_n}^{Fe,X}\right)\right\} \quad (1)$$

where $E_c(\Lambda_V^{Fe})$ and $E_c(\Lambda_X^{Fe,X})$ are the energies of crystals containing a vacancy and an interstitial X atom, respectively, and $E_c(\Lambda^{Fe})$ is the energy of the perfect crystal. The binding energy of one X atom in a VX_n complex, $E_b(VX_n)$, which is, in other words, the binding energy between an X atom and a VX_{n-1} complex, can be calculated as the difference between the total binding energies of VX_n and VX_{n-1}, i.e.

$$E_b(VX_n) = E_b^T(VX_n) - E_b^T(VX_{n-1}) \quad (2)$$

To obtain information on the origin of the total binding energy, we decompose the total binding energy into the distortion binding energy, $E_b^d(VX_n)$, and the electronic binding energy, $E_b^e(VX_n)$:

$$E_b^T(VX_n) = E_b^d(VX_n) + E_b^e(VX_{n-1}) \quad (3)$$

The distortion binding energy is the energy that can be gained by reducing the distortion in the host iron matrix when all the defects, i.e. one vacancy and n X atom(s), combine to form a complex. This can be written as

$$E_b^d(VX_n) = n \times E_d(\Lambda_X^{Fe}) + E_d(\Lambda_V^{Fe}) - E_d(\Lambda_{VXn}^{Fe}) \quad (4)$$

where $E_d(\Lambda_X^{Fe})$, $E_d(\Lambda_V^{Fe})$ and $E_d(\Lambda_{VXn}^{Fe})$ are the distortion energies due to an interstitial X atom, a vacancy and a VX_n complex, respectively. The distortion energy of configuration Λ_α^{Fe} is defined as

$$E_d(\Lambda_\alpha^{Fe}) = E_c(\Lambda_\alpha^{Fe}) - k \times E_{coh}^{Fe} \quad (5)$$

where k is the number of iron atoms in configuration Λ_α^{Fe}, and E_{coh}^{Fe} is the cohesive energy of pure Fe. On the other hand, the electronic binding energy is the difference in the energies of the Fe–X and X–X bonds before and after the formation of the VX_n complex. This is written as

$$E_b^e(VX_n) = E_b^{Fe-X}(VX_n) + E_b^{X-X}(VX_n) - n \times E_b^{Fe-X}(X) \quad (6)$$

where $E_b^{Fe-X}(VX_n)$, $E_b^{X-X}(VX_n)$ and $E_b^{Fe-X}(X)$ are the energies of Fe–X and X–X bonds in a crystal with a VX_n complex and Fe–X bond in a crystal with an interstitial X atom, respectively, and are defined as follows:

$$E_b^{Fe-X}(VX_n) = E_c(\Lambda_{VX_n}^{Fe}) + E_c(\Lambda_{VX_n}^{X}) - E_c(\Lambda_{VX_n}^{Fe,X}) \quad (7)$$

$$E_b^{X-X}(VX_n) = n \times E^C - E_c(\Lambda_{VX_n}^{X}) \quad (8)$$

$$E_b^{Fe-X}(X) = E_c(\Lambda_X^{Fe}) + E^C - E_c(\Lambda_X^{Fe,X}) \quad (9)$$

where E^C is the energy of a single X atom.

For substitutional solute atoms, the iron atom located at the first-nearest-neighbor (1NN) or second-nearest-neighbor (2NN) distance from the vacancy is replaced with the solute atom of interest, and then the crystal is relaxed in the same manner as for the interstitial solute atoms described above. The binding energy between a vacancy and a substitutional solute atom is calculated as

$$E_b(VY) = \left\{E_c\left(\Lambda_V^{Fe}\right) + E_c\left(\Lambda_Y^{Fe,Y}\right)\right\} - \left\{E_c\left(\Lambda_{VY}^{Fe,Y}\right) + E_c\left(\Lambda^{Fe}\right)\right\} \quad (10)$$

where Y is the solute atom.

3. Results and discussion

3.1. Verification of the calculations

We first calculated the vacancy and divacancy formation energies in bcc Fe to verify the accuracy of our calculations. The calculated values are compared in Table 1 with experimental data and the results of other calculations obtained using first-principles and empirical methods [5–8]. Our result for the vacancy formation energy is within the range of the scatter of the experimental data and slightly larger than the results of the other calculations. The binding energy of the divacancy at the 2NN distance is lower than that at the 1NN distance, which is consistent with the results of the other calculations. The magnitudes of the divacancy binding energies are also very similar among the calculations.

The main difference between our calculations and the other first-principles calculations is the cell relaxation. We relax the cell volume and cell shape, whereas other calculations were carried out under a constant-volume condition. To verify the effect of cell relaxation, we calculate the vacancy formation energy and *VC* binding energy for different supercell sizes of 54, 128 and 250 atoms as shown in Table 2. Brillouin zone integration is performed with a $5 \times 5 \times 5$ mesh for the 54-atom supercell calculation and with a $3 \times 3 \times 3$ mesh for the 128- and 250-atom supercell calculations. Vacancy formation energies converged rapidly to the supercell size for both the fully relaxed calculation and the constant-volume calculation. Both methods lead to similar satisfactory results for a small strain defect such as a vacancy. The vacancy formation energy in reference [5] is slightly smaller than the value we obtained. This difference originates from the pseudopotential method. The ultrasoft pseudopotential (USPP) method overestimates the magnetic moment and magnetization energy, particularly for the GGA method [4]. For the *VC* binding energy, the situation is different. The *VC* binding energy increases with supercell size and converges at a supercell size of 128 atoms in the fully relaxed calculation, while it decreases with supercell size and does not converge at a supercell size of 250 atoms in the constant-volume calculation. The *VC* binding energy obtained from the fully relaxed calculation is smaller than that obtained from the constant-volume calculation. As shown in Eq. (1), the total energy of interstitial C in the iron crystal is used for the reference energy. The distortion energy of the interstitial C causes this effect with changing supercell size. The energy difference obtained from the two calculations is 0.1 eV for the 128-atom supercell. The *VC* binding energy in reference [9] is 0.25 eV smaller than the value we obtained. This is due to the overestimation of magnetization energy by the USPP method.

Table 1
Vacancy and divacancy (first-nearest-neighbor (1NN) and second-nearest-neighbor (2NN)) formation energies in bcc Fe.

	Vacancy	Divacancy	
		(1NN)	(2NN)
EAM (Johnson and Oh)	1.73	0.16	0.22
US-GGA (PW91, const. vol.)[a]	2.09	0.17	0.23
US-GGA (PW91, const. vol.)[b]	2.02	0.15	0.29
SIESTA-GGA (PBE, const. vol.)[c]	2.07		
This work (PAW-PBE)	2.17	0.16	0.23
Experimental value[d]	2.0 ± 0.2		

[a] Ref. [5].
[b] Ref. [6].
[c] Ref. [7].
[d] Ref. [8].

Table 2
Vacancy formation energy and *VC* binding energy.

	PAW full relax.		PAW const. vol.		USPP const. vol.[a,b]	
	V	*VC*	*V*	*VC*	*V*	*VC*
54 atoms	2.15	0.56	2.15	0.74	1.93	0.44
128 atoms	2.17	0.59	2.17	0.69	2.02	0.47
250 atoms	2.17	0.60	2.16	0.66		

[a] Ref. [5].
[b] Ref. [9].

3.2. Binding energies of VX_n complexes

The total binding energies of VX_n, where X is either C or N, with n from 1 to 6, are shown in Table 3. Different topological configurations exist for VX_n for n from 2 to 4, as schematically shown in Fig. 1. Energy diagrams showing the total binding energies of one X atom to a VX_{n-1} complex are shown in Fig. 2, and the decomposition of the total binding energy into the distortion relaxation energy and the electronic interaction energy is shown in Fig. 3.

Regarding the carbon atoms, a carbon atom located at the substitutional site of the vacancy gives a negative total binding energy of −0.18 eV, indicating that this configuration is unstable. The interatomic distance between the carbon atom and the 1NN Fe atom is 2.34 Å in this configuration, which is too far for an electronic bond to form between the carbon and iron atoms. On the other

Table 3
Total binding energy of VX_n (X = C and N) complexes in electron volts.

Configuration	This work		USPP-PW91 (constant volume)[a]	
	C	N	C	N
VX (O site)	0.59	0.86	0.44	0.74
VX (substitution site)	−0.18	−0.81	−0.33[b]	−0.88[b]
VX_2 (1D)	1.53	1.83	1.07	1.54
VX_2 (2D)	1.56	0.73	1.50	0.46
VX_3 (2D)	1.82	0.55	1.84	−0.11
VX_3 (3D)	0.74	−0.02	0.72	−0.46
VX_4 (2D)	1.35	−1.11		
VX_4 (3D)	−0.44	−1.00		
VX_5	−1.25	−3.20		
VX_6	−5.20	−6.11		

[a] Ref. [9].
[b] Results for 54-atom supercell.

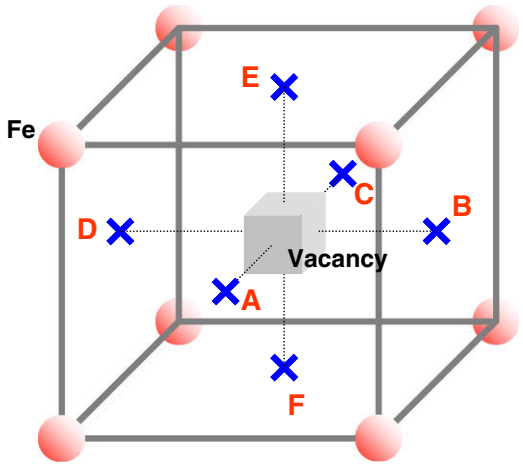

VX_n	name	example
VX_2	1D	A – C
VX_2	2D	A – B
VX_3	2D	A – B – C
VX_3	3D	A – B – E
VX_4	2D	A – B – C – D
VX_4	3D	A – B – C – E

A –F : six Octahedral (O) sites of the vacancy

Fig. 1. Definition of VX_n complex structures. For example, the complex with a vacancy and three carbon atoms located at the O-sites A, B and E is called VX_3 (3D).

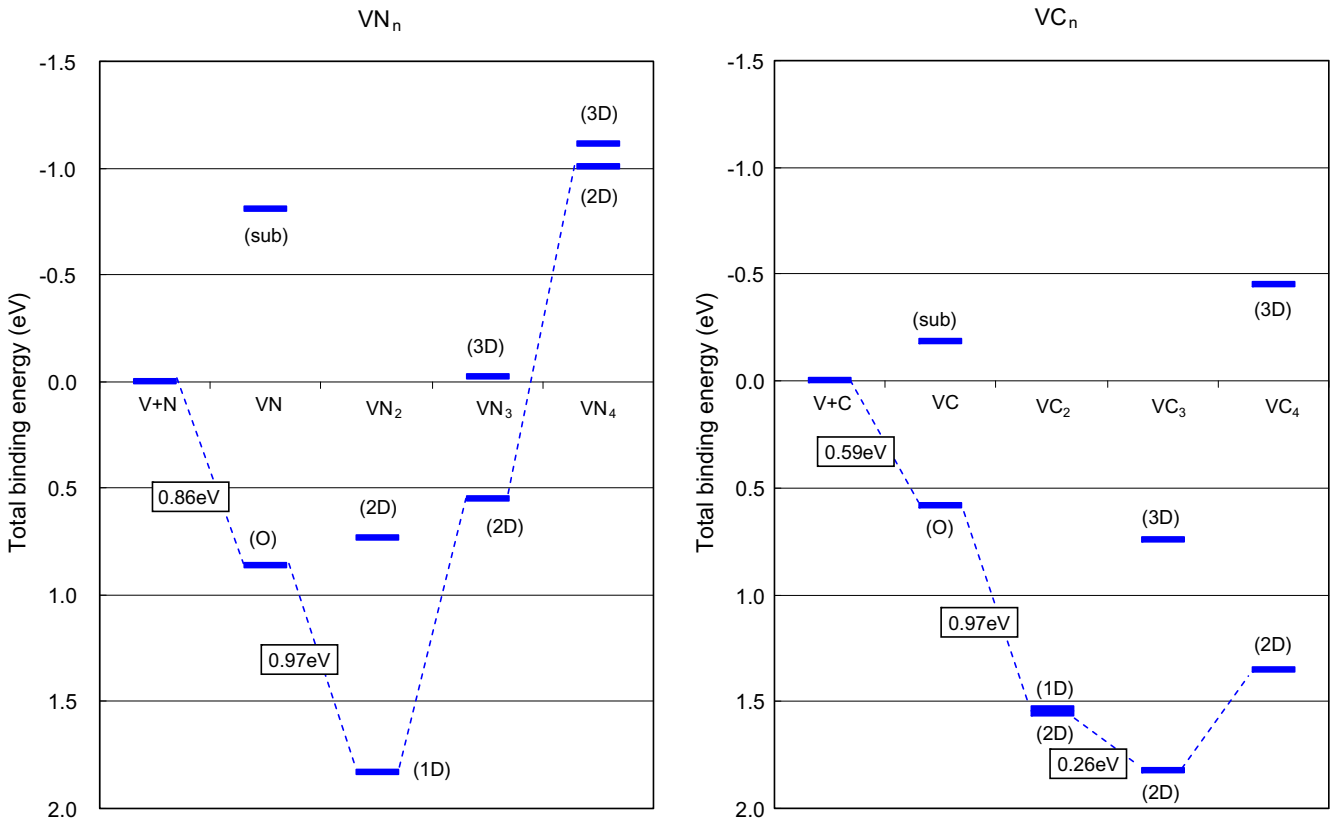

(a) VN_n complex (b) VC_n complex

Fig. 2. Total-binding-energy diagrams of: (a) VC_n complex and (b) VN_n complex. The differences between the neighboring energies are the binding energies of a single X atom to the complex.

hand, a carbon atom occupying the octahedral site (O-site) of the vacancy has a strong binding energy of 0.59 eV. We also attempted to calculate the total binding energy of the VC complex with a carbon located at the T-site, but this configuration always relaxes to the VC (O-site) configuration. When we increase the number of carbon atoms in the VC_n complex, the total binding energy also increases with n when $n \leq 3$, but the total binding energy of VC_4 (3D) is smaller than that of VC_3 (2D) although its value is still positive. The total binding energies are negative

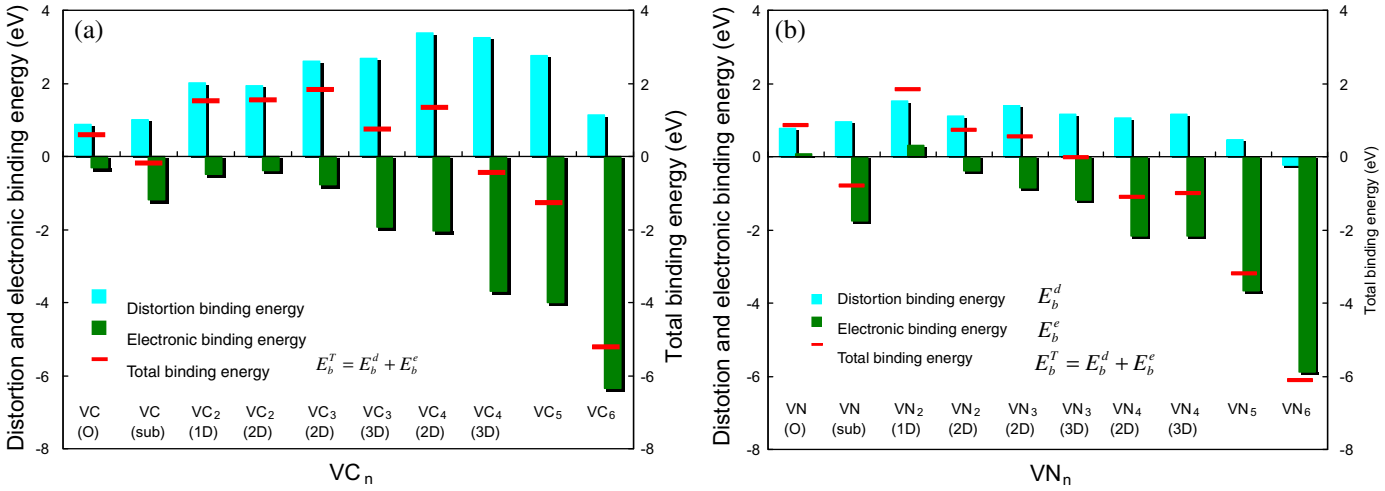

Fig. 3. Decomposition of the total binding energy into distortion binding energy and electronic binding energy for (a) VN_n and (b) VC_n. Total binding energies are shown as red horizontal bars.

for VC_5 and VC_6 as well as for VC_4 (3D), and these configurations are clearly unstable. It is interesting to note that the total binding energy is dependent on configuration for configurations with the same number of carbon atoms. The energy difference between VC_2 (1D) and VC_2 (2D) is relatively small, but the difference between VC_3 (2D) and VC_3 (3D) is as large as 1.08 eV. This is more pronounced for the case of four-carbon complexes. The total binding energy of VX_4 (2D) is 1.35 eV, while VX_4 (3D) has a negative value of −0.44 eV, resulting in a very large difference of 1.79 eV.

The binding energies of a carbon in VC_n, i.e. the binding energies between VC_{n-1} and C, are positive for n from 1 to 3 as shown in Fig. 2. The binding energy between VC and C in VC_2 (2D) has a maximum value of 0.97 eV, while that between C and VC_2 (2D) in VC_3 (2D) has the smallest value of 0.24 eV. Although the total binding energy of VC_4 (2D) is positive, the binding energy between C and VC_3 in this configuration has a negative value of −0.47 eV, indicating that VC_4 (2D) preferentially forms to be VC_3 (2D) and one interstitial carbon by emitting a carbon atom from the complex to reduce the total energy. Note that this process is still a thermally activated process because the dissociation energy of VC_4 (2D) has a positive value of 0.40 eV, which is the sum of the binding energy of −0.47 eV and the migration energy of a carbon atom of 0.87 eV.

The stability of VN_n complexes is slightly different from that of VC_n. The VN (O-site) complex has a very high binding energy of 0.86 eV, while the VN (substitution) complex has a very negative binding energy of −0.81 eV. The VN (T-site) configuration is unstable, as can be seen in the VC complex, and the configuration relaxes to the VN (O-site) configuration. The total binding energy of VN_2 (1D) is as high as 1.83 eV, but the VN_2 (2D) configuration has a much lower binding energy of 0.73 eV, which is less than half that of VN_2 (1D). The total binding energy of VN_3 is either negative for VN_3 (2D) or positive but less than that of VN_2 (1D) for VN_3 (3D). All the VN_n configurations with n from 4 to 6 have a negative total binding energy, indicating that these configurations are unstable. We also calculated the binding energies of a single nitrogen to VN_n complexes as shown in Fig. 2. Both VN and VN_2 give very high energies of 0.86 eV and 0.97 eV, respectively. For VN_n with n greater than 2, however, the binding energy becomes negative.

The total binding energies of VC_n and VN_n are compared with the results obtained by Domain et al. [9]. The results are consistent for VC_n complexes except for the VC_2 (1D) configuration, for which we obtained a much larger binding energy. For VN_n complexes, the results again appear to be consistent, but our results give slightly larger binding energies in general. For the VN_3 (3D) configuration, our calculation gives a positive and nontrivial total binding energy while the calculation in reference [9] gives a negative binding energy. The differences between our calculations and those in reference [9] are the boundary conditions, pseudopotential and the cutoff energy of the plane wave. As described in Section 3.1, the USPP method overestimates the magnetization energy and magnetic moment. In the case of the VN_3 (3D) configuration, the constant-volume calculation indicates a large distortion. In Ref. [9], the total binding energy of VN_3 (3D) for a 54-atom supercell is −0.38 eV and that for a 128-atom supercell is −0.11 eV. The total binding energy may become positive in a large supercell.

3.3. Energy decomposition of VX_n clusters

3.3.1. VC_n complexes

The origin of the total binding energies can be determined by decomposing them into distortion and electronic

binding energies, as defined in Section 2. The calculated energy decomposition for VC_n and VN_n complexes is shown in Fig. 3. For the VC_n complexes shown in Fig. 3a, one can see that the distortion binding energy increases with n up to $n = 4$ but decreases for $n = 5$ and 6. The distortion energies are always positive, indicating that the strain induced by the separated vacancy and carbon atoms is always relaxed and reduced when they agglomerate to form a VC_n complex. The magnitude of the distortion binding energy depends on the number of carbon atoms but does not depend strongly on their configuration for VC_n complexes with the same number of carbon atoms.

On the other hand, the electronic binding energy is always negative. For complexes with more than one carbon atom, the electronic binding energy monotonically decreases with the number of carbon atoms. One can also see that the electronic binding energy depends not only on the number of carbon atoms in VC_n complexes but also on their positions.

For VC complexes, the electronic binding energy of VC (substitution) is much smaller than that of VC (O-site). The carbon atom in VC (substitution) cannot form very strong bonds with the 1NN iron atoms because the atomic distance between the carbon atom and the iron atoms is 2.34 Å, which is too large for a bond to be formed in contrast with the VC (O-site) configuration, where the carbon–iron atomic distance is only 1.73 Å. Owing to this very low electronic binding energy in the VC (substitution) complex, its total binding energy is negative, where as it is positive in the VC (O-site) complex.

In the case of VC_2 complexes, the electronic binding energies do not differ greatly between VC_2 (1D) and VC_2 (2D), and thus the total binding energies for these complexes are very similar. In the case of VC_3 and VC_4 complexes, however, the magnitude of the electronic binding energy significantly depends on the carbon positions in the complexes. In both VC_3 and VC_4 complexes, the 3D configurations, in which the carbon atoms are located more closely to each other than in the 2D configurations, have much lower electronic binding energies than the 2D configurations, resulting in the lower total binding energies of the 2D configurations in both VC_3 and VC_4 complexes. This is caused by the formation of carbon–carbon bonds in the VC_n complexes. To clarify this situation, further decomposition of the electronic binding energy in VC_n complexes is shown in Fig. 4a. Since Fig. 4 shows the contribution of the electronic bonds to the electronic binding energies of VC_n complexes, the energies of the electronic bonds formed in the reference state, i.e. the interstitial carbon state in Fig. 4a, are shown as negative values. When the carbon atoms are at the interstitial atom positions in the iron matrix, iron and carbon atoms form strong bonds between them. However, when carbon atoms are located in a vacancy to form a VC_n complex, carbon–carbon bonds are formed between the carbon atoms separated by a short distance in the VC_n complex. The formation of carbon–carbon bonds weakens the iron–carbon bonds, and thus the electronic binding energies in the 3D configurations of VC_3 and VC_4, where carbon atoms are more closely packed, are lower than those in the 2D configurations.

These observations of the electronic bond formation explain the behavior of the distortion binding energy from a different viewpoint. The strain field around a carbon atom in the iron matrix is caused by the interaction between the carbon atom and the 1NN iron atoms. In the VC_n complexes, the formation of carbon–carbon bonds weakens the bonds between the iron and carbon atoms, and this results in the relaxation of the strain field around the carbon atoms in VC_n complexes.

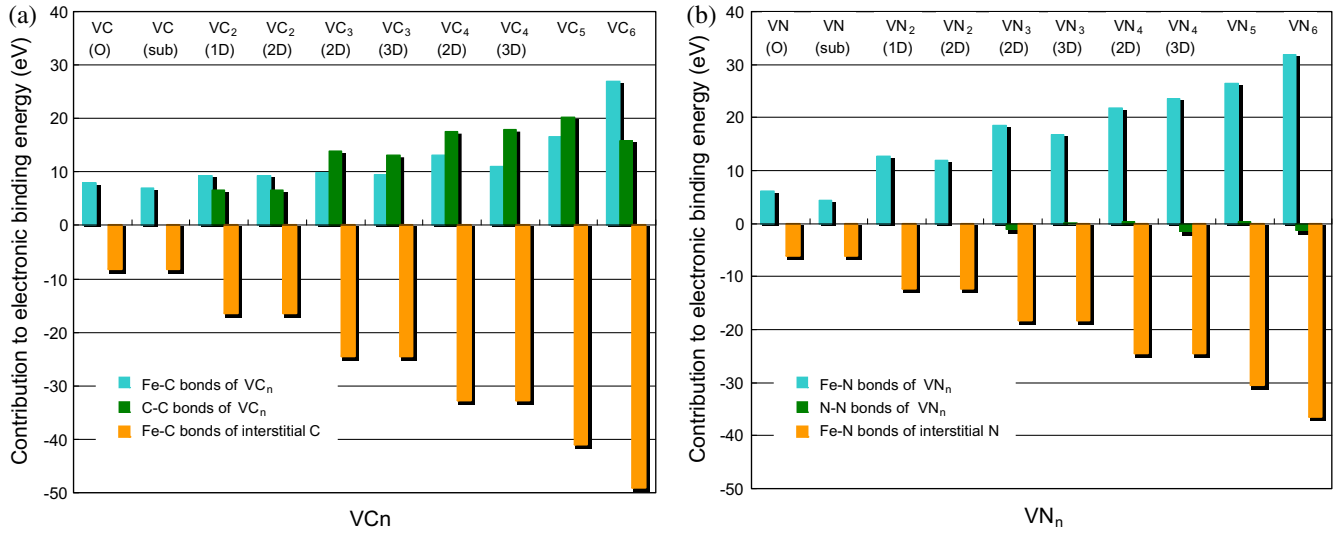

Fig. 4. Decomposition of electronic binding energies into the contributions of Fe–X bonds and X–X bonds of VX_n complex and Fe–X bonds of interstitial X for (a) VC_n and (b) VN_n. Since the definition of the electronic binding energy is the difference between the binding states of VX_n and interstitial X, the contributions of Fe–X bonds of the interstitial X are shown as negative values.

3.3.2. VN_n complexes

For the VN_n complexes, the situation is very different. The distortion binding energies in Fig. 3b do not increase greatly with the number of nitrogen atoms, i.e. the magnitudes of the distortion binding energies are very similar among the VN_n complexes with n from 1 to 4, very small for VN_5 and negative for VN_6. This means that the formation of VN_n complexes does not result in a large energy gain from the viewpoint of distortion. On the other hand, the electronic binding energy monotonically decreases with increasing number of nitrogen atoms from 2 to 6. Most of the electronic binding energies are negative, but the values for the VN (O-site) and VN_2 (1D) configurations are positive. The electronic binding energy for VN (substitution) is negative and very large in magnitude. The difference between of the electronic binding energies of the VN_2 (1D) and VN_2 (2D) complexes is not trivial, while the electronic binding energies of VN_3 and VN_4 do not depend strongly on whether the nitrogen atom configuration is 2D or 3D, i.e. both VN_3 (2D) and VN_3 (3D), and VN_4 (2D) and VN_4 (3D) have very similar electronic binding energies. These observations for VN_2, VN_3 and VN_4 complexes are very different from those for VC_n complexes.

The decomposition of the electronic binding energies shown in Fig. 4b and the comparison of Fig. 4a and b can help us understand the above results. At first glance it is clear that there is almost no contribution of nitrogen–nitrogen bonds to the electronic binding energies of the VN_n complexes with n from 2 to 6. In the case of the VN (O-site) configuration, the small positive electronic binding energy observed in Fig. 3b is due to the fact that the contribution of the iron–nitrogen bonds is slightly larger than that in the interstitial nitrogen configuration. This is different from the case of the VC (O-site) configuration, and is primarily owing to the difference in the number of bonds allowed for carbon and nitrogen atoms. The reason for the smaller energy of iron–nitrogen bonds in the VN (substitution) configuration is the same as that in the VC (substitution) configuration.

In the case of the VN_2 (1D) configuration, there are no nitrogen–nitrogen bonds in the complexes. The two nitrogen atoms are almost independent of each other, and the energy of the iron–nitrogen bonds is almost twice that in the VN (O-site) configuration. Thus, the positive electronic binding energy in the VN_2 (1D) configuration is almost as large as that in the VN (O-site) configuration. In the VN_2 (2D) configuration, the contribution of the iron–nitrogen bond is slightly smaller than that in the VN_2 (1D) configuration because two nitrogen atoms bond to one iron atom. As a result, the electronic binding energy becomes negative, in contrast to that in the VN_2 (1D) configuration. For the VN_3 and VN_4 configurations, the energies of iron–nitrogen bonds are slightly affected by the nitrogen configuration, but when the iron–nitrogen bonds become stronger, the nitrogen–nitrogen bonds have negative energies to compensate for the increased energy of the iron–nitrogen bonds, and thus the total electronic binding energies are almost unchanged.

In summary, the decomposition of the electronic binding energy clearly shows that the binding state between the atoms is very different for VN_n and VC_n, in particular, no nitrogen–nitrogen bond is formed in the VN_n complexes. In some cases, the nitrogen–nitrogen interactions are repulsive. This should again be closely related to the insensitivity of the distortion binding energy to the type of VN_n complex. The lack of formation of nitrogen–nitrogen bonds means that the relaxation of the iron lattice around the VN_n complex cannot occur, and thus the distortion binding energy does not increase with n. Eventually the total binding energy becomes very different from that of VC_n complexes.

3.4. Experimental results on VC_n binding energies

V–C binding energies of 0.41–1.1 eV have been obtained in various experiments [10–13]. Arndt and Damask has obtained a value of 0.41 eV by calorimetry, which is consistent with the values of 0.41 eV and 0.48 eV obtained by the classical molecular dynamics studies of Johnson et al. and Rosato, respectively [14,15]. Vehanen et al. [13] has obtained a V–C binding energy of 0.85 eV by positron lifetime measurement and they argued that Arndt and Damask's value is the VC–C binding energy. Frank et al. obtained a value of 0.97 eV by considering internal friction [12], and Takaki et al. obtained a value of 1.1 eV by considering recovery resistivity [10]. On the other hand, the results of Tapasa et al.'s [16] simulation based on rate theory and Vehanen et al.'s recovery stage of 350 K can be reproduce using a V–C binding energy of 0.44–0.5 eV. Our calculated value is 0.59 eV, which is slightly larger than Tapasa et al.'s result.

Frank et al. also obtained the VC–C and VC_2–C binding energies by considering internal friction. The VC–C binding energy is 0.42 eV and the VC_2–C binding energy is 0.24 eV [12]. Our calculated VC–C and VC_2–C binding energies are 0.97 eV and 0.24 eV, respectively. The results of Tapasa et al.'s simulation based on rate theory and the VC_2 dissociation state at 480 K can be reproduced using a VC–C binding energy of 0.8–1.0 eV. This is consistent with our results. The calculated VC_2–C binding energy is in good agreement with the experimental value.

3.5. Substitutional elements

The calculated total binding energies of VY (Y = 3d transition metal and Si, P, S, Mo) in iron together with experimental values and other calculated values are shown in Table 4 [17–19]. The binding energies of VY are typically approximately 0.2–0.3 eV except for the cases of Sc and S. These values are smaller than the VC and VN binding energies. In the cases of Ni and Co, the 2NN VY binding energies are larger than those of the 1NN binding energies. This agrees with the experimental result that the 2NN binding energy is larger than the 1NN binding energy in Ni [18].

Table 4
Total, distortion and electronic binding energies of VX (X = 3d transition metal, Si, P, S and Mo) in electron volts.

Solute	Sc	Ti	V	Cr	Mn	Co	Ni	Cu	Zn	Si	P	S	Mo
This work	0.63	0.22	0.04	0.05	0.16	0.10	0.19	0.24	0.33	0.29	0.36	0.53	0.33
Experiment [a,b]		0.16	<0.11	<0.11	0.15	0.14	0.22	0.14		0.23			
USPP-const. vol. [c]					0.12		0.18	0.19		0.24			
Distortion binding energy	0.36	0.06	0.00	0.00	0.00	0.00	0.01	0.02	0.06	0.02	0.02	0.03	0.07
Electronic binding energy	0.27	0.16	0.04	0.05	0.16	0.10	0.18	0.22	0.27	0.27	0.34	0.50	0.26

[a] Ref. [17].
[b] Ref. [18].
[c] Ref. [19].

For the other elements, 1NN binding energies are larger than the 2NN binding energies. Our calculated values are consistent with the experimental values and other calculated values.

To determine the origin of the total binding energy, we also decompose the total binding energies into distortion and electronic binding energies. The decomposed binding energies are shown in Table 3. Except for the case of Sc, the distortion binding energies are very small and less than 0.7 eV. Although Mo is known to be an oversized element in iron, the distortion binding energy is only 0.07 eV. Only Sc has a large distortion binding energy (0.36 eV), which is why Sc has a large VY binding energy of 0.63 eV. In the case of interstitial elements, VC and VN have large distortion energies of approximately 1 eV. This is also why VC and VN have large binding energies.

The binding volume can be calculated in the same manner as the binding energy of Eq. (10). The binding volume, $Vo_b(VY)$, can be written as

$$Vo_b(VY) = \left\{Vo\left(\Lambda_V^{\mathrm{Fe}}\right) + Vo\left(\Lambda_Y^{\mathrm{Fe},Y}\right)\right\} - \left\{Vo\left(\Lambda_{VY}^{\mathrm{Fe},Y}\right) + Vo\left(\Lambda^{\mathrm{Fe}}\right)\right\} \quad (11)$$

where $Vo(\Lambda_V^{\mathrm{Fe}})$ denotes the supercell volume of the crystal containing a vacancy and $Vo(\Lambda_Y^{\mathrm{Fe},Y})$ denotes the supercell volume of the crystal containing a vacancy and element Y. The binding volume dependence of the binding energy of V-solute elements is shown in Fig. 5. The total VY binding energy increases linearly with increasing VY binding volume, except in the case of Sc. The change in the formation volume means the change in volume when VY forms. In the case of 3d transition metals, the distortion binding energy is small. The electronic binding energy is related to the change in formation volume. The electronic bonding surrounding VY changes as the formation volume changes. The VY (Y = 3d transition metal) distortion binding energy is 0.06 eV or less except for the case of Sc. The electronic binding energy is the major part of the total VY binding energy for the 3d transition metals.

In the cases of Si, P and Mo, the total VY binding energy is approximately 0.4 eV. This is slightly larger than those for 3d transition metals. The distortion binding energies of Si, P and Mo are 0.07 eV or less. The total binding energy of the VS complex is 0.53 eV, which is larger than

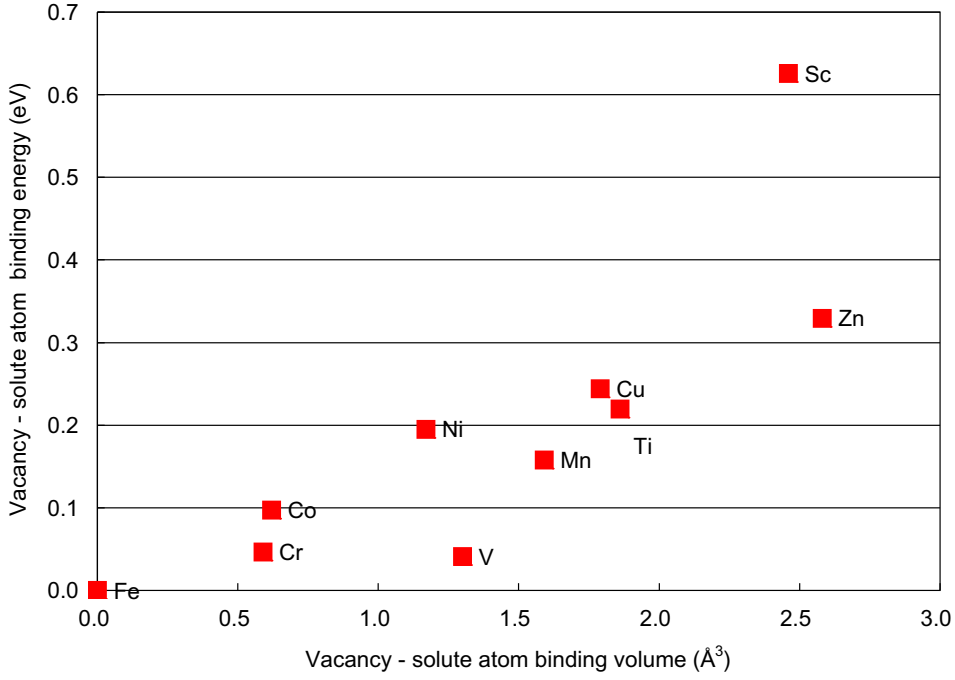

Fig. 5. Binding volume dependence of binding energy of V-solute elements.

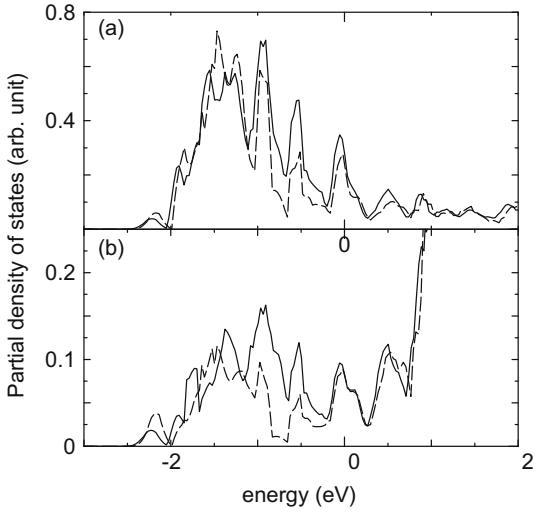

Fig. 6. Partial densities of states (PDOS) of S and 1NN iron atom to S in Fe–S (dashed line) and Fe–V–S complex (solid line): (a) PDOS of S atom, (b) PDOS of Fe atom.

that of other substitute solution elements. The distortion binding energy of VS is small (0.03 eV) and the electronic binding energy is the largest component of the total binding energy. The partial densities of states of S atom and the 1NN iron atom to the S atom in Fe–S and Fe–V–S are shown in Fig. 6. These partial densities of states of the VS complex are larger than those in Fe–S solution. Thus, the electronic bonding is stronger in the case of Fe–V–S.

4. Summary

We have performed first-principles calculations of vacancy (V) and vacancy-solute element complexes in bcc Fe. In VC_n complexes of bcc iron, VC_3 (2D) is the most stable complex and the total binding energy is largest (0.97 eV) between VC_2 (1D) and VC. In VN_n complexes, VN_2 is the most stable complex and the total binding energy is largest (also 0.97 eV) between VN_2 (1D) and VN. These large total binding energies originate from the matrix distortion energy of the interstitial elements. We also calculated the binding energies of vacancy–substitutional solute elements (3d transition metals and Mo, Si, P, S) in bcc iron. These total binding energies are typically approximately 0.2–0.3 eV, and are not as large as those for interstitial solute elements.

References

[1] Kresse G, Furthmuller J. Phys Rev B 1996;54:11169.
[2] Perdew JP, Burke K, Ernzerhof M. Phys Rev Lett 1996;77:3865.
[3] Blochl PE. Phys Rev B 1994;50:17953.
[4] Kresse G, Joubert D. Phys Rev B 1999;59:1758.
[5] Tateyama Y, Ohno T. Phys Rev B 2003;67:174105.
[6] Domain C, Becquart CS. Phys Rev B 2002;65:024103.
[7] Fu C-C, Willaime F. Phys Rev Lett 2004;92:175503.
[8] De Schepper L, Segers D, Dorikens-Vanpaet L, Dorikens M, Knuyt G, Stals L, et al. Phys Rev B 1983;27:5257.
[9] Domain C, Becquart CS, Foct J. Phys Rev B 2004;69:144112.
[10] Takaki S, Fuss J, Kugler H, Dedek U, Schultz H. Radiat Eff 1983;79:87.
[11] Arndt RA, Damask AC. Acta Metall 1964;12:341.
[12] Frank W, Weller M, Diehl J, Seeger A. Mater Sci Forum 1987;15–18:685.
[13] Vehanen A, Hautojarvi P, Johansson J, Yli-Kauppila J, Moser P. Phys Rev B 1982;25:762.
[14] Johnson RA, Dines GJ, Damask AC. Acta Metall 1964;12:1215.
[15] Rosato V. Acta Metall 1989;37:2759.
[16] Tapasa K, Barashev AV, Bacon DJ, Osetsky Yu-N. Acta Metall 2007;55:1.
[17] Doyama M. Nihon Kinzoku Gakkai Kaihou 1986;25:808.
[18] Möslang A, Albert E, Recknagel E, Weidinger A, Moser P. Hyperfine Interact 1984;17–19:255.
[19] Vincent E, Becquart CS, Domain C. Nucl Instrum Meth Phys Res B 2005;228:137.